Glycobiology vol. 24 no. 11 pp. 1036–1049, 2014
doi:10.1093/glycob/cwu069
Advance Access publication on July 6, 2014

NMR characterization of the binding properties and conformation of glycosaminoglycans interacting with interleukin-10

Georg Künze[1,2], Jan-Philip Gehrcke[3], M Teresa Pisabarro[3], and Daniel Huster[2,4]

[2]Institute of Medical Physics and Biophysics, University of Leipzig, Härtelstraße 16/18, D-04107 Leipzig, Germany; [3]Structural Bioinformatics, BIOTEC TU Dresden, Tatzberg 47-51, D-01307 Dresden, Germany; and [4]Department of Chemical Sciences, Tata Institute of Fundamental Research, Homi Bhabha Road, Colaba, Mumbai 400 005, India

Received on May 2, 2014; revised on July 1, 2014; accepted on July 1, 2014

The cytokine interleukin-10 (IL-10) is an important regulator of the host immune system with both pro- and anti-inflammatory functions. Glycosaminoglycans (GAGs) play a decisive role in the biology of many growth factors, e.g., for receptor binding or protection from proteolytic degradation. GAGs of the extracellular matrix inhibit IL-10 signaling, however, the molecular mechanism is so far unknown. Here, we studied the interaction between GAGs and IL-10 using a combination of nuclear magnetic resonance (NMR) spectroscopy and computer simulations. The binding region of a set of heparin and chondroitin sulfate GAG disaccharides with varying sulfation pattern were determined by saturation transfer difference (STD) NMR spectroscopy. From the initial growth rate of the STD amplification factor binding affinities were determined and K_D values in the low millimolar to micromolar range were obtained. We observed the highest binding affinity to IL-10 with fully sulfated heparin; however, a hyaluronan hexasaccharide did not exhibit binding, which suggests that GAG sulfation is necessary for interaction with IL-10. For octasaccharides or longer GAGs, a cooperative binding behavior was observed, which could indicate simultaneous interaction with both dimer subunits of IL-10. Finally, structural information about the bound GAG was exemplarily obtained for a heparin tetrasaccharide fragment (ΔUA,2S-GlcNS,6S-IdoA,2S-GlcNS,6S) using transferred NOESY experiments, proton–proton scalar couplings and molecular dynamics simulations. The overall backbone conformation is only slightly changed in the presence of IL-10 and the conformational equilibrium between $^1C_4$ chair and ^2S_o skew-boat structure of the internal iduronic acid residue is preserved.

Keywords: glycosaminoglycans / interleukin-10 / molecular dynamics / NOE / STD spectroscopy

Introduction

The immune response bears the intrinsic risk of an immune-mediated inflammatory damage to the host tissue. The cytokine interleukin (IL)-10 is a key regulator of the innate and adaptive immune system, which prevents an overwhelming immune reaction and tissue damage (Sabat et al. 2010). IL-10 inhibits the synthesis of pro-inflammatory cytokines (e.g., IL-1, IL-6, IFN-γ and TNF-α) (Fiorentino et al. 1989) and of cell surface molecules (e.g., MHC class II proteins) involved in antigen recognition and T-cell stimulation (Moore et al. 1993). Thereby, cellular immune responses mediated, e.g., by macrophages or T-cells are inactivated.

IL-10 is a domain swapped, symmetric homodimer and this specific protein fold is shared with other cellular and viral homologues of IL-10 (Zdanov 2004). Transduction of the extracellular IL-10 signal through the cell membrane is accomplished by two receptor chains, IL-10R1 and IL-10R2, which activate the intracellular JAK–STAT pathway. The ternary IL-10 signaling complex is thereby assembled in a sequential manner: first by binding of IL-10 to IL-10R1 with high affinity (~500 pM) (Tan et al. 1995) and second by low-affinity interactions between IL-10R2 and the preformed binary complex (Yoon et al. 2006).

However, interaction of IL-10 with the cell surface is not limited to receptor binding alone but was also shown for components of the extracellular matrix, especially for glycosaminoglycans (GAGs) (Salek-Ardakani et al. 2000). GAGs are a family of linear negatively charged polysaccharides consisting of repeating disaccharide units in which one sugar residue is a hexuronic acid (either D-glucuronic acid [GlcA] or L-iduronic acid [IdoA]) and the other one is an amino hexose (either D-glucosamine [GlcN] or D-galactosamine [GalN]). GAGs include hyaluronan (HA), heparan sulfate (HS), heparin, keratan sulfate (KS), chondroitin sulfate (CS) and dermatan sulfate (DS). Except for HA, which is synthesized as free polymer, all GAGs are initially linked to core proteins forming proteoglycans. GAGs are highly negatively charged due to the addition of sulfate groups. Both the degree and position of sulfation can show a high heterogeneity between different GAG subgroups as well as within the same GAG chain, a fact known as sulfation code. For example, HS shows a multi domain structure consisting of highly sulfated, L-iduronic acid containing S domains, less sulfated, *N*-acetyl-D-glucosamine containing NA domains and finally, mixed domains acting as transition zones between S and NA domains (Gallagher et al. 1990; Gallagher 1997).

GAGs and proteoglycans are found in the extracellular matrix of all animal tissues, in the basement membrane, on

[1]To whom correspondence should be addressed: Tel: +49-341-9715744; Fax: +49-341-9715709; e-mail: georg.kuenze@medizin.uni-leipzig.de

cellular membranes or in the secretory granules of many cell types (Gallagher 1989; Prydz and Dalen 2000). Besides their role as scaffold substances, e.g., in cartilage, GAGs can directly affect the function of many cellular proteins like cytokines, chemokines and growth factors (Gandhi and Mancera 2008). For example, binding to cell surface proteoglycans can form tissue-specific reservoirs of cytokines and growth factors (Roberts et al. 1988; D'Amore 1990) or gradients of chemokines, which are presented to migrating cells (Handel et al. 2005; Johnson et al. 2005). Furthermore, interaction with GAGs has also been shown to protect proteins against proteolytic degradation (Pratta et al. 2003; Sadir et al. 2004) and to regulate receptor binding (Gallagher and Turnbull 1992; Clarke et al. 1995).

Several observations suggest that GAGs can play an important role in the biology of IL-10 as well, similar to the mechanisms mentioned above. Binding of the cytokine to the cell surface of mouse derived macrophages was detected, which could not be attributed to the IL-10 receptor but must have arisen from another molecule, possibly from a GAG (Fleming and Campbell 1996). Indeed, binding of IL-10 to heparin was experimentally confirmed by surface plasmon resonance (Salek-Ardakani et al. 2000). Furthermore, the effect of GAGs on IL-10 signaling was investigated. Heparin, HS, CS and DS were all shown to deteriorate the IL-10 induced expression of CD16 and CD64 by monocytes and macrophages (Salek-Ardakani et al. 2000). The strongest inhibitory effect was therefore observed for heparin and HS with IC_{50} values of 100–500 µg/mL. Considerably higher concentrations of CS and DS were required with IC_{50} values of 2000–5000 µg/mL. However, experiments were performed with quite heterogeneous GAG preparations from animal sources with undefined specification of GAG chain length, sulfation pattern or uronic acid epimerization as in the case of heparin. A detailed analysis of the structural principles that form the basis of GAG-IL-10 interactions was therefore limited, and the mechanism by which GAGs influence IL-10 activity still remains unknown.

In the present study, we performed saturation transfer difference (STD) nuclear magnetic resonance (NMR) experiments of a series of GAG oligosaccharides with murine IL-10 to gain insights into the binding properties of the complex. Thereby, protons in close contact with the protein were identified for heparin and CS-derived disaccharides and for the heparin tetrasaccharide ΔUA,2S-GlcNS,6S-IdoA,2S-GlcNS,6S. Furthermore, binding affinity was quantified and its dependence on GAG sulfation and chain length was tested. In addition, for octasaccharides or longer GAGs a cooperative binding behavior was observed. Finally, information on the bioactive conformation of the strongest binder, heparin, was obtained from transferred nuclear Overhauser enhancement (trNOE) NMR experiments and proton–proton ^{3}J couplings. The heparin structure was calculated by applying NOE-restrained molecular dynamics (MD) simulations and revealed only minor conformational changes of the heparin backbone upon binding to IL-10.

Our results suggest a possible role of extracellular matrix GAGs on the biological functions of IL-10, e.g., for signaling and bioavailability. Furthermore, this information can be used for biotechnological applications of GAGs and IL-10, e.g., for the design of tissue-like matrix materials in regenerative medicine. Modification with GAG derivatives can improve engraftment of the artificial tissue and release of IL-10 from the matrix into the surroundings can inhibit inflammation and support tissue regeneration.

Experimental procedures

Materials

Heparin disaccharides I-S (ΔUA,2S(1 → 4)GlcNS,6S), II-S (ΔUA(1 → 4)GlcNS,6S), III-S (ΔUA,2S(1 → 4)GlcNS), IV-S (ΔUA(1 → 4)GlcNS), I-A (ΔUA,2S(1 → 4)GlcNAc,6S) and I-H (ΔUA,2S(1 → 4)GlcN,6S) were purchased from Sigma-Aldrich (Taufkirchen, Germany). CS disaccharides C2S (ΔUA,2S(1 → 3)GalNAc), C4S (ΔUA(1 → 3)GalNAc,4S), C6S (ΔUA(1 → 3)GalNAc,6S), C2,4S (ΔUA,2S(1 → 3)GalNAc,4S), C2,6S (ΔUA,2S(1 → 3)GalNAc,6S), C4,6S (ΔUA(1 → 3)GalNAc,4S,6S) and C2,4,6S (ΔUA,2S(1 → 3)GalNAc,4S,6S) and heparin derived tetra-(ΔUA,2S(1 → 4)GlcNS,6S(1 → 4)IdoA,2S(1 → 4)GlcNS,6S), hexa-(ΔUA,2S(1 → 4)GlcNS,6S(1 → 4)[IdoA,2S(1 → 4)GlcNS,6S]$_2$), octa-(ΔUA,2S(1 → 4)GlcNS,6S(1 → 4)[IdoA,2S(1 → 4)GlcNS,6S]$_3$) and decasaccharides (ΔUA,2S(1 → 4)GlcNS,6S(1 → 4)[IdoA,2S(1 → 4)GlcNS,6S]$_4$) were obtained from Carbosynth (Compton, UK). All other used chemicals were purchased from Sigma-Aldrich (Taufkirchen, Germany) or Carl Roth (Karlsruhe, Germany).

Protein expression and purification

Mouse IL-10 was prepared as previously described (Künze et al. 2013). In short, IL-10 was expressed in *Escherichia coli* Rosetta(DE3) and was refolded from insoluble inclusion body material. To prevent incorrect disulfide bond formation a C149Y IL-10 mutant was prepared with improved refolding yield but comparable activity to the wild-type protein (Ball et al. 2001). Subsequently, IL-10 was purified by nickel affinity chromatography and gelfiltration.

NMR experiments

NMR experiments were recorded on a Bruker Avance III 600 MHz spectrometer (Bruker Biospin GmbH Rheinstetten, Germany) equipped with a 5 mm inverse triple resonance probe with z-gradient and on a Bruker Avance II 700 MHz spectrometer using a 5 mm triple resonance cryoprobe with z-gradient. The Bruker software Topsin™ 2.1. was used for data acquisition and spectra processing.

Carbohydrate ^{1}H and ^{13}C resonances were assigned using standard ^{1}H–^{1}H correlation spectroscopy, ^{1}H–^{1}H total correlation spectroscopy (TOCSY), ^{1}H–^{1}H rotating-frame nuclear Overhauser effect spectroscopy (ROESY) and ^{1}H–^{13}C heteronuclear single quantum coherence (HSQC) experiments (Wider et al. 1984; Kay et al. 1992). Typical ^{1}H and ^{13}C 90° pulse lengths were 8.8 and 12 µs, respectively. In TOCSY experiments, spin-locking was obtained with an MLEV-17 sequence (Bax and Davis 1985) with a mixing time of 90 ms and a field strength of 9.6 kHz. ^{1}H–^{13}C HSQC spectra were recorded with z-gradients for coherence selection (Schleucher et al. 1994) and GARP decoupling (Shaka et al. 1985) during acquisition. All spectra were recorded at 25°C. ^{1}H chemical shifts were referenced to the external standard 2,2-dimethyl-2-silapentene-5-sulfonate (DSS), whereas ^{13}C chemical shifts were calibrated

indirectly. Chemical shift assignments of all used GAGs can be found in Supplementary data.

STD NMR experiments

For STD NMR experiments, samples contained 40 μM IL-10 in 10 mM potassium phosphate (pH 7.0) and 50 mM NaCl (99.8% D_2O). To improve saturation transfer from the protein to the carbohydrate protons, all spectra were measured at 10°C. A pseudo-2D version of the STD NMR sequence was used for the interleaved acquisition of on- and off-resonance spectra. For selective saturation of the protein, a cascade of 50 E-Burp-shaped pulses with a length of 50 ms each and an interpulse delay of 1 ms was used. The on-resonance frequency was set to 0.202 ppm and the off-resonance pulse was applied at 30 ppm. For suppression of the residual water signal, a Watergate sequence was used. Typically, STD spectra were acquired with a 50- to 100-fold excess of ligand, a saturation time of 4 s, 256 scans and 16K complex points. Prior to Fourier transformation FIDs were multiplied by an exponential line broadening function of 1 Hz. For the heparin tetrasaccharide, STD effects were measured with an STD-HSQC experiment using the natural abundance of ^{13}C. The spectrum was acquired with a saturation time of 3 s, 3072 scans and 4K and 64 data points in the direct and indirect dimensions, respectively.

To identify those ligand protons that are in close contact to IL-10, their individual T_1 relaxation was taken into account since otherwise ligand relaxation has a substantial influence on the magnitude of the observed STD effects. Therefore, T_1 relaxation times were measured with a 1D inversion recovery experiment (see Supplementary data for details).

Binding isotherms of individual GAGs were determined using the initial growth rate approach of the STD amplification factor (STD-AF) (Angulo et al. 2010), in which the initial slope of the STD-AF at time zero is extrapolated. The STD-AF is defined as the product of the STD intensity η_{STD} and the excess of ligand ($\varepsilon = [L]_0/[P]_0$) (Mayer and Meyer 2001):

$$\text{STD-AF} = \varepsilon \cdot \frac{(I_0 - I_{Sat})}{I_0} = \varepsilon \cdot \eta_{STD}, \qquad (1)$$

where I_0 is the intensity of the reference spectrum and I_{Sat} is the intensity of the on-resonance spectrum.

For STD buildup, curves saturation times were chosen at 1, 2, 3 and 5 s. The total duration of each experiment was 6 s. Initial slopes of the STD-AF were obtained from an exponential fit of the STD-AF buildup curve:

$$\text{STD-AF}(t) = a(1 - \exp(-bt)). \qquad (2)$$

The product of both coefficients a and b represents the initial slope STD-AF_0. Dissociation constants (K_D) were obtained from a fit of the STD-AF_0 values as a function of ligand concentration with a 1:1 binding model:

$$\text{STD-AF}_0([L]) = \frac{[P] + [L] + K_D}{2} - \sqrt{\left(\frac{[P] + [L] + K_D}{2}\right)^2 - [P][L]}, \qquad (3)$$

where [P] and [L] are the concentrations of the protein and ligand, respectively. Furthermore, binding curves were analyzed in terms of cooperativity and binding stoichiometry using a simple Hill-equation:

$$\text{STD-AF}_0([L]) = \frac{\text{STD-AF}_{max} \cdot [L]^n}{K_D + [L]^n}. \qquad (4)$$

Here, the exponent n is termed the Hill coefficient. Nonlinear least-squares fitting was performed with Origin 6.0 (MicroCal. Inc.).

trNOESY and ROESY NMR experiments

In the case of trNOESY and ROESY NMR experiments, samples contained 100 μM IL-10 and a 20-fold excess of heparin disaccharide or tetrasaccharide in 10 mM potassium phosphate (pH 7.0) and 50 mM NaCl (99.8% D_2O). Phase-sensitive NOESY and ROESY experiments were acquired at 600 MHz at 25°C with 16K and 256 data points in the direct and indirect dimension, respectively. Water suppression was achieved with a Watergate W5 sequence (Liu et al. 1998). NOESY mixing times ranged from 100 to 800 ms, and the ROESY mixing time was set to 150 or 300 ms with a spinlock field of 2500 Hz.

Structure calculation of free and IL-10-bound heparin tetrasaccharide

NMR derived proton–proton distances. NOE cross-peak intensities for the IL-10-bound and ROE cross-peak intensities for the free heparin tetrasaccharide fragment (ΔUA,2S-GlcNS, 6S-IdoA,2S-GlcNS,6S) were measured from experiments with 150 ms mixing time, at which the buildup curve is in the linear region and contributions from spin diffusion are expected to be small. This was also confirmed by theoretical simulations of the NOESY and ROESY spectra at the experimental conditions using the program Noemol (Forster and Mulloy 1994). To further exclude effects from spin diffusion, a transferred ROESY experiment was performed for heparin in the presence of IL-10. Here, cross-peaks with the same sign as the diagonal signals can indicate spin diffusion.

^1H–^1H distances were calculated from cross-peak intensities assuming a $1/r^6$ distance dependence between interacting protons and were calibrated using the pairs of vicinal protons (H2–H4 or H3–H5) of the GlcNS,6S ring with a known distance of 2.55 Å in the $^4C_1$ chair conformation. A tolerance interval of ±0.3, ±0.6 and ±1.0 Å was used as upper and lower limit restraint for experimental distances of <2.0, 2.0–4.0 and >4.0 Å, respectively.

NOE-restrained MD. We performed simulated annealing MD simulations for heparin structure determination based on the distance restraints obtained experimentally. The simulations were conducted using Amber 12 (Case et al. 2012), and based on atomic parameters given by the GLYCAM 06 g force field (Kirschner et al. 2008). Structure determination was performed in a two-step protocol, first by structure optimization in implicit solvent, and subsequent refinement in explicit solvent. The two stages were repeated 100 times, yielding an ensemble of structure models (see Supplementary data for methodological details).

Results

Identification of GAG protons in close contact to IL-10

Using one- and two-dimensional STD NMR experiments, those protons in GAG di- and tetrasaccharide molecules that form close contacts to IL-10 were identified. The GAG monosaccharide composition and sulfation pattern is illustrated in Figure 1. Because GAG oligosaccharides were prepared by enzymatic digestion, the non-reducing terminal uronic acid becomes unsaturated. Although di- and tetrasaccharides cover only a short part of the naturally occurring long GAG chains, they provide several advantages. They are available as pure compounds with defined degrees and patterns of sulfation. In contrast, higher molecular-weight fractions of sulfated GAGs commercially available are produced from natural sources and can often not be purified to high homogeneity. This often impedes an unambiguous interpretation of experimental results. Furthermore, severe signal overlap in the NMR spectra of long carbohydrates prevents unambiguous signal assignment and accurate quantification of STD effects. Finally, pronounced STD effects were already observed for GAG disaccharides suggesting the disaccharide to make considerable interaction with IL-10. The observation that GAG disaccharides and oligosaccharides occupy the same binding region of IL-10 as found from chemical shift perturbations of the protein backbone (see Supplementary data, Figure S1 for details) lets us conclude that information obtained on the binding properties of GAG disaccharides are transferable to longer GAGs.

The reference and the STD NMR spectrum of the C2,4,6S disaccharide are shown in Figure 2, and the $^{1}H–^{13}C$ HSQC reference and the STD spectrum of heparin tetrasaccharide are displayed in Figure 3. To deduce the relative proximity of the ligand protons from the STD spectra, STD signals were integrated and STD intensities were corrected for the T_1 relaxation rate of the respective protons of the free ligand. T_1 relaxation times varied by a factor of 6 at which H6 protons of the glucosamine (heparin) or galactosamine (CS) ring showed the fastest relaxation (T_1 ~0.5 s) and the H4 proton in the 4,5-unsaturated uronic acid ring having the slowest relaxation (T_1 ~ 3–3.5 s). Relaxation times along with the ^{1}H and ^{13}C chemical shifts of all investigated GAGs are reported in Supplementary data, Tables SI–SVI. STD effects were observed for all GAGs except for HA, indicating that it does not bind IL-10 (Supplementary data, Figure S2). HA exhibits only one carboxylate group per disaccharide unit but no sulfate group. This observation suggests that sulfation is necessary for IL-10-GAG binding. Furthermore, only weak STD effects were observed for the C6S and for the heparin I-H disaccharide, which did not allow for accurate quantification of their STD intensities. A summary of the determined STD effects is given in Figure 4. Obviously, the strongest STD effects were found for protons near the sulfate groups,

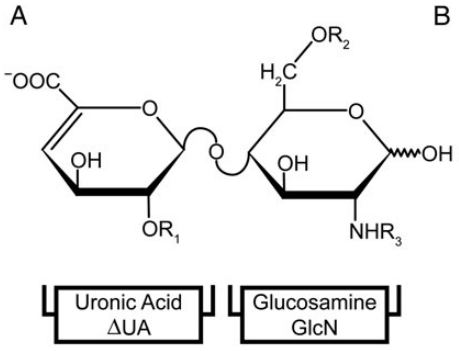

Heparin Disaccharide	R_1	R_2	R_3
I-S	$-SO_3^-$	$-SO_3^-$	$-SO_3^-$
II-S	-	$-SO_3^-$	$-SO_3^-$
III-S	$-SO_3^-$	-	$-SO_3^-$
IV-S	-	-	$-SO_3^-$
I-A	$-SO_3^-$	$-SO_3^-$	$-COCH_3$
I-H	$-SO_3^-$	$-SO_3^-$	$-NH_3^+$

Chondroitin Disaccharide	R_1	R_2	R_3
C2S	$-SO_3^-$	-	-
C4S	-	$-SO_3^-$	-
C6S	-	-	$-SO_3^-$
C2,4S (CS B)	$-SO_3^-$	$-SO_3^-$	-
C2,6S (CS D)	$-SO_3^-$	-	$-SO_3^-$
C4,6S (CS E)	-	$-SO_3^-$	$-SO_3^-$
C2,4,6S	$-SO_3^-$	$-SO_3^-$	$-SO_3^-$

Fig. 1. Substitution pattern of the GAG disaccharides used in this study. GAG disaccharides were prepared by lyase digestion. This results in the formation of a 4,5-unsaturated uronic acid ring (ΔUA), which is β(1–4)-linked to glucosamine in heparin disaccharides (**A**) or β(1–3)-linked to *N*-acetylgalactosamine in CS disaccharides (**C**). The carboxylate group in ΔUA is positioned in the ring plane as indicated by an oblique bond orientation in the chemical structures. Substitutions in heparin (**B**) can occur at position O2 of ΔUA and at N2 and O6 of GlcN, whereas in CS disaccharides (**D**) sulfations are linked to position O2 of ΔUA and to O4 and O6 of GalNAc. Naturally occurring CS is mostly monosulfated but polysulfated regions can exist too, which have often functional relevance (Deepa et al. 2002).

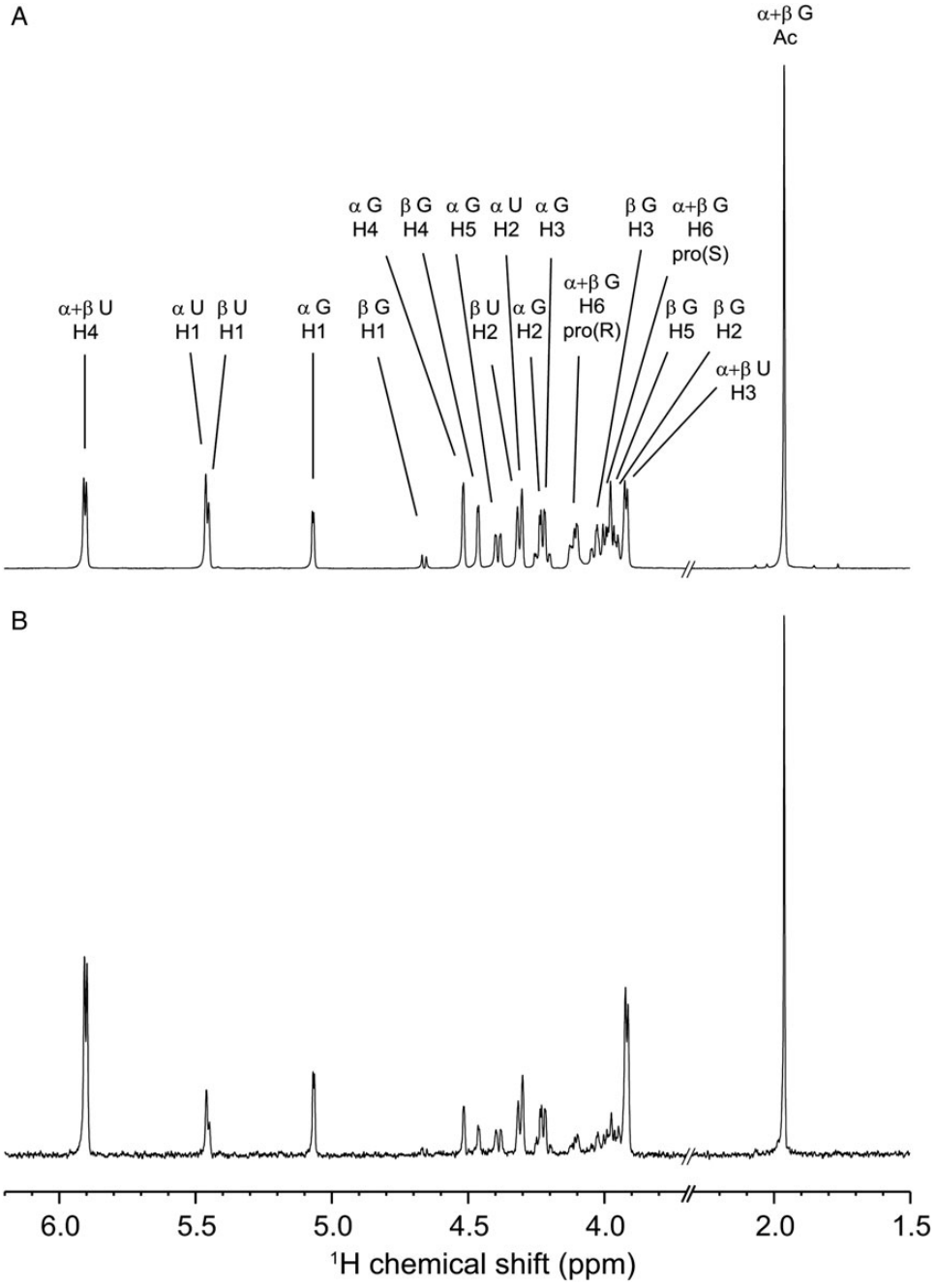

Fig. 2. (**A**) 1D ^{1}H reference and (**B**) STD NMR spectrum (6× magnification) of C2,4,6S (ΔUA,2S(1 → 3)GalNAc,4S,6S) at 600 MHz, 10°C, a saturation time of 4 s and a protein–ligand ration of 1:100. Signals arising from the 4,5-unsaturated uronic acid (ΔUA) or *N*-acetylgalactosamine (GalN) residue are labeled with "U" or "G", respectively. α or β denotes the respective anomeric form of C2,4,6S.

i.e., protons H2, H4, H5, H6pro(R) and H6pro(S) of glucosamine or galactosamine and for protons H1 and H2 of the uronic acid. This observation identifies sulfate groups as important interaction points and is in agreement with other known protein–GAG complexes, where binding is mostly driven by electrostatic interactions between positively charged protein residues and the negatively charged sulfate groups of the GAGs (Faham et al. 1996; Li et al. 2004; Esko and Linhardt 2009; Pichert et al. 2012). Additional strong STD effects were observed for protons H3 and H4 next to the anionic carboxylate group of the unsaturated uronic acid ring. Finally, also the methyl protons of the acetamide group in the glucosamine and galactosamine showed dominant STD effects.

Binding affinity of IL-10 and GAGs as a function of GAG sulfation and chain length

The influence of GAG sulfation on IL-10 binding strength was further analyzed by measuring the binding affinity of differently sulfated heparin and CS disaccharides. Direct evaluation of the

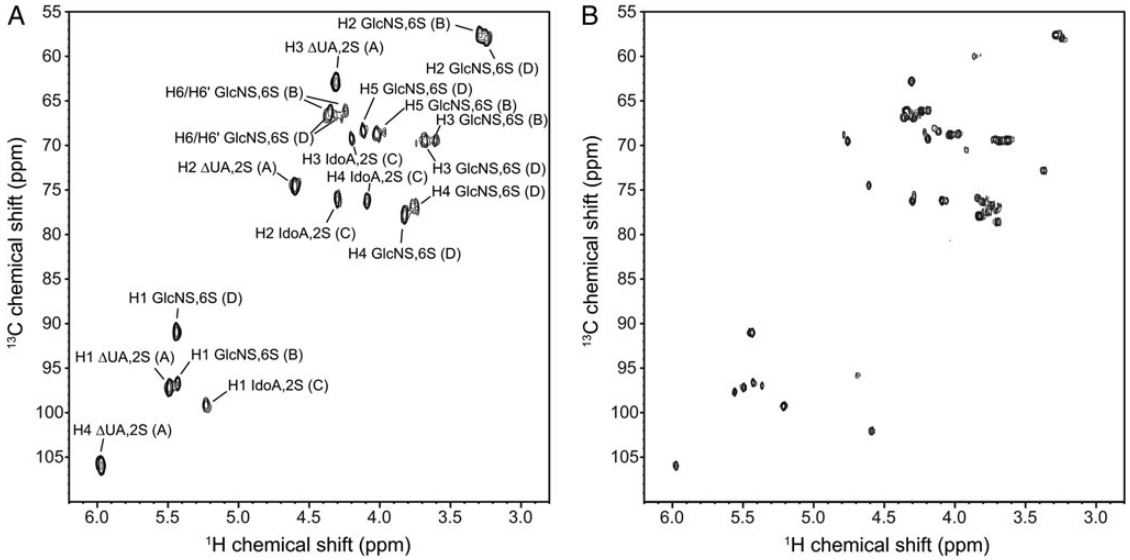

Fig. 3. (**A**) 2D ^{1}H–^{13}C STD and (**B**) reference NMR spectrum of heparin tetrasaccharide at 700 MHz, 10°C, a saturation time of 3 s and a 50-fold excess of ligand using natural abundance of ^{13}C. In (**A**), proton signals are labeled with their respective monosaccharide residues: 4,5-unsaturated uronic acid (ΔUA,2S), 2-O-sulfo-iduronic acid (IdoA,2S) and 2-*N*,6-*O*-disulfo-glucosamine (GlcNS,6S). Sugar rings are labeled with (A)–(D) starting at the non-reducing end of the tetrasaccharide.

dissociation constant from variation of the STD value with the protein–ligand ratio is not feasible because of the complex dependence of the STD intensity on various experimental factors such as saturation time, longitudinal relaxation of ligand signals and lifetime of the protein–ligand complex. We have therefore used the initial growth rate approach in which the growth rate of the STD-AF was measured and extrapolated to the point of zero saturation time. Under these circumstances, virtually no ligand turnover takes place and fast ligand–protein rebinding that influences STD signal intensity is avoided. Figure 5 shows the binding curves for selected heparin and CS disaccharides, and Table I summarizes the measured K_D values for all used GAGs assuming a 1:1 binding model. IL-10 is a homodimeric protein with a 2-fold rotational symmetry. Therefore, we assume that it can provide two structurally equivalent GAG-binding sites. Since no evidence for binding site cooperativity in case of the studied GAG disaccharides as well as for the heparin tetra- and hexasaccharide was found, we further conclude that binding of those small GAGs to each of the sites occurs independently. Therefore, a 1:1 binding model (one GAG molecule and one IL-10 monomer) seems to be valid.

Among the heparin disaccharides, heparin I-S showed the highest affinity ($K_D \sim 0.2$ mM). Removal of the 2-O-sulfation (heparin II-S) and of the 6-O-sulfation (heparin III-S) led to only a slight decrease in binding affinity resulting in K_D values of 0.7 and 1.8 mM, respectively (Table I). In contrast, N-desulfation at the GlcN,6S ring, i.e., in heparin I-H, led to a dramatic drop in the interaction strength as indicated by a right shift of the binding curve (Figure 5). Thus, the K_D value of heparin I-H could not accurately be determined within the available concentration range since no saturation of IL-10 by heparin I-H was reached. The observed decrease in affinity is probably due to the exposure of a primary amino group, which is positively charged at physiological conditions and can cause repulsive interactions with cationic protein residues. While we cannot distinguish whether it is the local positive charge or the missing sulfate that prohibits binding, this observation points out the crucial role of charged groups for protein–GAG interactions. Interestingly, acetylation of the amino group, as in heparin I-A, yielded a comparable affinity ($K_D \sim 0.6$ mM) as for the full sulfated heparin I-S. That means, it could partly recover the effect of N-desulfation and functional groups at the N2-position other than sulfates are also tolerated by IL-10.

Within the studied CS disaccharides, a clear correlation between strength of binding to IL-10 and degree of sulfation was observed as well. The trisulfated C2,4,6S has the lowest K_D value (0.3 ± 0.1 mM). Removal of one sulfate group led to a decrease in affinity in the order 2-O-desulfation (C4,6S with $K_D = 1.4 \pm 0.3$ mM), 4-O-desulfation (C2,6S with $K_D = 2.3 \pm 0.3$ mM) and 6-O-desulfation (C2,4S with $K_D = 3.2 \pm 1.1$ mM). However, differences in the binding affinity between these disaccharides were still very small and we could not reveal a predominant role of one specific sulfation position. Finally, for single sulfated CS compounds, a further decrease in interaction strength was observed. C2S and C4S have a comparable affinity ($K_D = 4.7 \pm 3.4$ and 5.3 ± 1.8 mM, respectively). On the contrary, C6S has a slightly weaker affinity ($K_D = 12.4 \pm 4.6$ mM) than the latter two disaccharides. This could suggest a minor contribution of 6-O-sulfation to GAG-IL-10 binding compared with the 2-O-sulfation and the 4-O-sulfation, which would be consistent with the observed lower inhibitory effect of C6S on the IL-10 signaling activity measured in cell culture experiments (Salek-Ardakani et al. 2000). However, experimental errors for C6S and C2S are quite large, mainly because no complete saturation could be reached for both ligands during titration up to concentrations of 15 and 4 mM, respectively. Furthermore, doubling of the K_D value still means only a small change in the free energy of binding. Thus, for CS disaccharides, we cannot find a

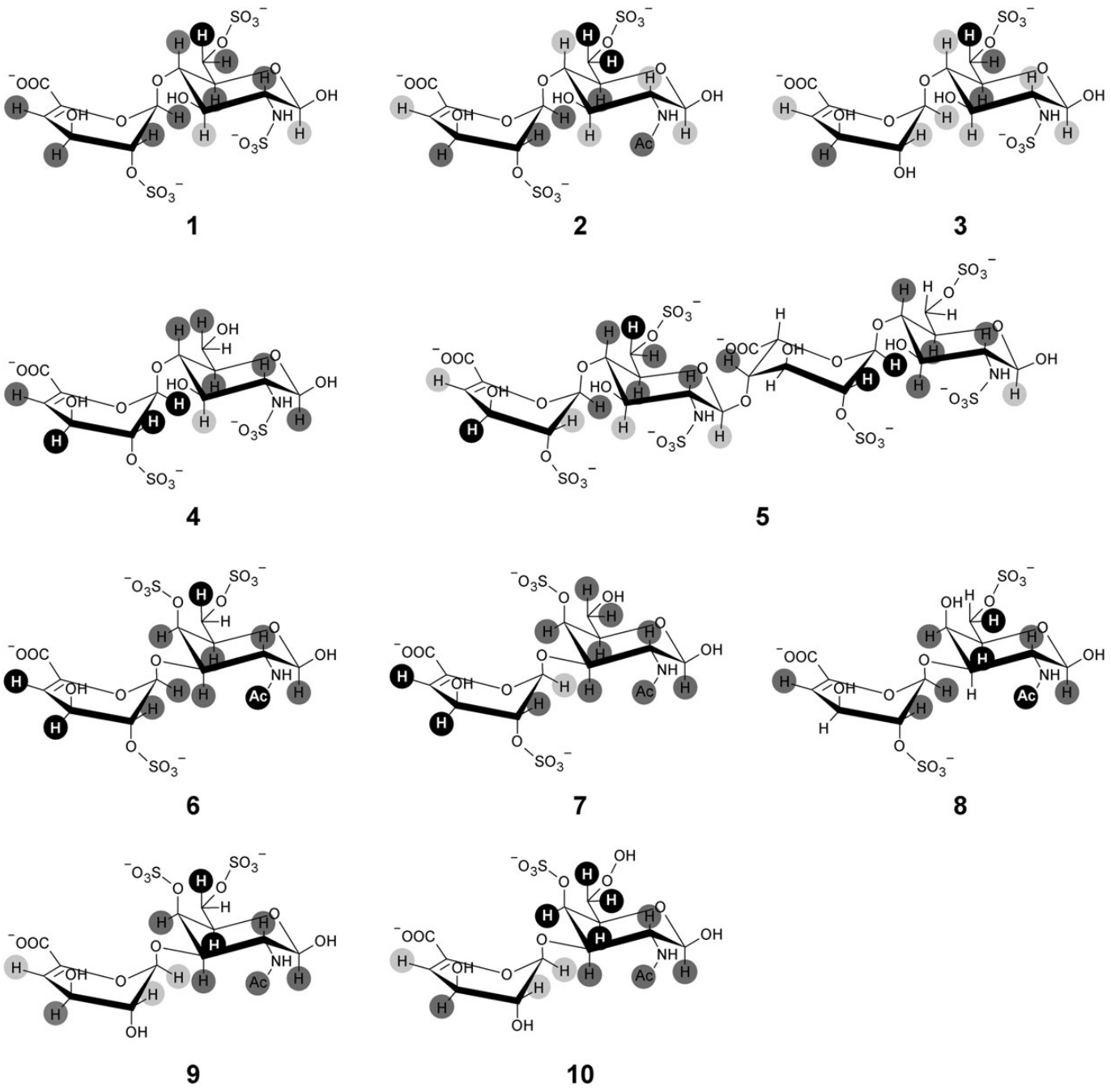

Fig. 4. Chemical structures of used heparin and CS carbohydrates and their binding regions: heparin I-S (**1**), I-A (**2**), II-S (**3**), III-S (**4**), heparin tetrasaccharide (**5**), C2,4,6S (**6**), C2,4S (**7**), C2,6S (**8**), C4,6S (**9**) and C4S (**10**). STD effects were obtained at a ligand to protein molar ratio of 50:1 for heparin saccharides, of 300:1 for C4S and of 100:1 for all other CS disaccharides. The relative STD effects were normalized to the highest STD signal for each ligand itself. Dark, medium and light gray circles indicate strong (>75%), medium (75–40%) and weak (<40%) STD effects, respectively. Protons with no circles were not analyzed due to spectral overlap.

clear role of the O-sulfation pattern as determinant of GAG binding. Rather the sulfation degree seems to be more important as found also for the heparin disaccharides.

GAGs are natural polymers, and elongation of the GAG chain can allow binding of additional disaccharide repeating units that provide more molecular contacts and can lead to an enhancement of their binding strength – a principle known as avidity. Indeed, for heparin molecules longer than a tetramer a clear left shift of the titration curve was found (Figure 6). The heparin hexasaccharide has a K_D value of 77 ± 19 μM and for the octa- and decasaccharide K_D values of 20 ± 9 and 11 ± 7 μM were determined, respectively. Similarly, a decrease of the maximal STD enhancement for longer heparin oligosaccharides also indicated a higher binding affinity of those

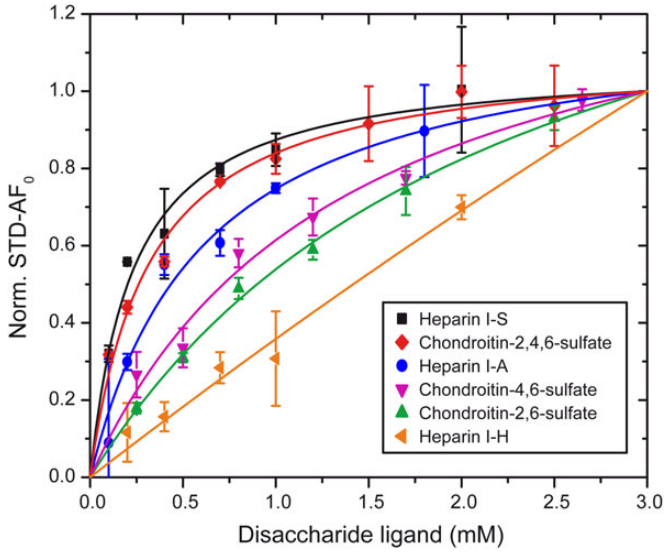

Fig. 5. Binding curves of selected GAG disaccharides as obtained from the initial growth rates of the STD amplification factor. The STD signal of proton H4 of the 4,5-unsaturated uronic acid unit (ΔUA) was analyzed for every GAG compound. Error bars for each titration point were obtained from the fit of the STD build up curve to an exponential function using the Levenberg–Marquet algorithm. STD-AF_0 values were fitted to a one site binding model. Dissociation constants (K_D) are given in Table I.

Table I. Dissociation constants (±SE) of CS disaccharides, heparin disaccharides and heparin oligosaccharides measured from the initial growth rate of the STD amplification factor at 10°C in 10 mM potassium phosphate (pH 7.0), 50 mM NaCl (99.8% D_2O)

CS disaccharide		Heparin disaccharide		Heparin oligosaccharide	
K_D ± SE (mM)		K_D ± SE (mM)		K_D ± SE (μM)	
C2S	4.7 ± 3.4	I-S	0.2 ± 0.0	Di	233 ± 40
C4S	5.3 ± 1.8	II-S	0.7 ± 0.4	Tetra	298 ± 42
C6S	12.4 ± 4.6	III-S	1.8 ± 0.2	Hexa	77 ± 19
C2,4S	3.2 ± 1.1	I-A	0.6 ± 0.1	Octa	20 ± 9
C2,6S	2.3 ± 0.3	I-H	n.d.[a]	Deca	11 ± 7
C4,6S	1.4 ± 0.3				
C2,4,6S	0.3 ± 0.1				

[a]n.d., not determined.

compounds (Supplementary data, Figure S3). This can be explained by the lower exchange rate, which leads to less saturated ligand molecules per time unit. Our data further suggest that the binding stoichiometry is changed for heparin molecules longer than a hexasaccharide. First, ligand saturating concentrations are reduced in the case of the octa- and decasaccharide as indicated by a left shift of the turning point in the binding curve (Figure 6). Second, a steeper slope of those binding curves, which can be displayed in a half-logarithmic scale (Supplementary data, Figure S4), argues in favor of a mode of positive cooperativity. We determined a Hill coefficient of 2.0 and 1.8 for the octa- and decasaccharide, respectively. In the case of strong cooperativity, the Hill coefficient equals the number of binding sites. Our observations can be explained by simultaneous binding of

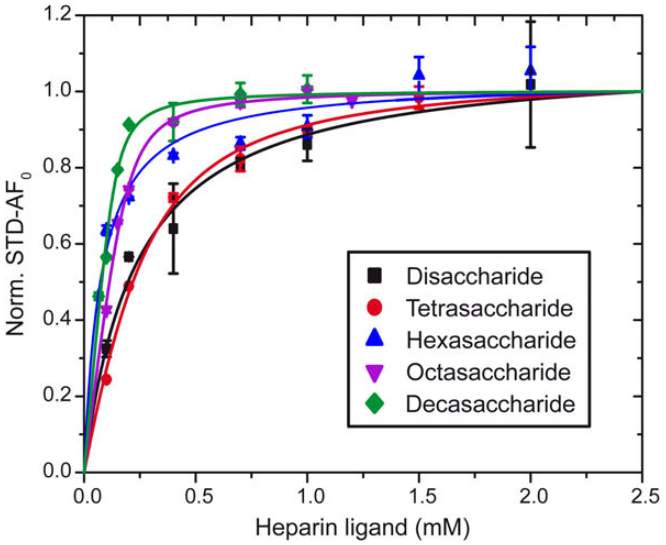

Fig. 6. Binding curves of heparin compounds with increasing chain length. As in Figure 5, the STD signal of H4 of the first 4,5-unsaturated uronic acid ring (ΔUA) was used to calculate initial growth rates of the STD amplification factor. Error bars indicate the error of the nonlinear least-squares fitting of the STD build up with the Levenberg–Marquet algorithm.

one heparin molecule to both IL-10 subunits. Interaction with the first monomer can favor binding to the second subunit, e.g., due to spatial restriction of the ligand molecule. Thus, affinity to the second binding site is greatly enhanced as reflected by positive cooperativity. Finally, if binding to the second subunit is fast, the protein exists in equilibrium only in two states: unbound or with both binding sites occupied. Then our interpretation of the Hill coefficient as number of binding sites is also valid.

NOESY and ROESY spectra of IL-10-bound GAGs

To investigate the conformation of a GAG molecule bound to IL-10, we have performed trNOE experiments with a heparin tetrasaccharide fragment (ΔUA,2S(1 → 4)GlcNS,6S(1 → 4) IdoA,2S(1 → 4)GlcNS,6S). For longer heparin molecules with identical repeating units, signal overlap is problematic and impedes the chemical shift assignment of each individual sugar ring. Furthermore, discrimination of NOEs arising solely from the protein-bound or unbound form becomes ambiguous because of the same sign of NOE cross-peaks in both forms. We found that under the chosen experimental conditions, the heparin hexasaccharide showed negative NOEs in the presence and absence of IL-10. The medium to low affinity of the ligand corresponds to a fast exchange between the protein-binding site and solution, which is why the NOESY spectrum of the heparin hexasaccharide represents an overlay of both forms. To dissect the pure protein-bound form one would need to apply a different isotopic labeling scheme of the protein or sugar together with isotope-edited and/or filtered NMR experiments.

In contrast, NOEs of the heparin tetrasaccharide in the free state were close to zero and did not interfere with signals of the bound state. At 150 ms mixing time, only some positive NOEs were observed between protons H2 and H3, H4 and H5 of

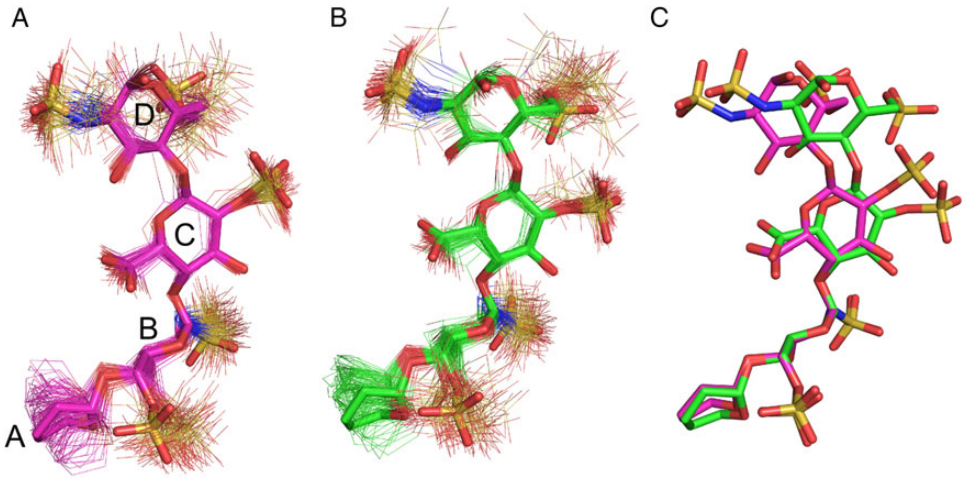

Fig. 7. Heparin structure models obtained from trNOE data and simulated annealing simulations. (**A**) Structure model ensemble for the unbound case (ring identifiers in capital letters). (**B**) Structure model ensemble for the bound case. (**C**) The representative structure for both, the unbound (carbons in magenta) and bound (carbons in green) ensembles, aligned on ring B. The ensemble representatives are shown in thick sticks. Functional groups of ring A and hydrogens are not shown for clarity. Atoms are colored by type (oxygen: red, nitrogen: blue, sulfur: yellow).

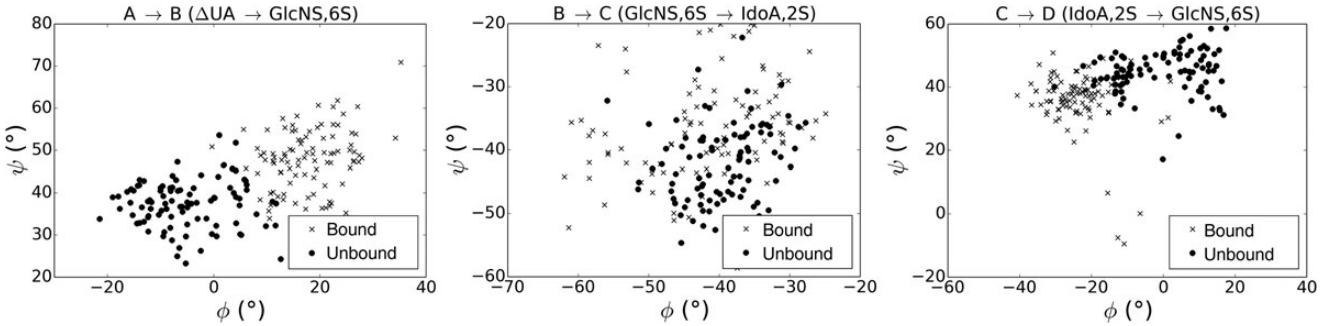

Fig. 8. Glycosidic linkage torsional angle distributions of heparin structure model ensembles obtained from NMR distance restraints and simulated annealing simulations. Data comparing the bound and unbound state are shown individually for each linkage in the heparin tetrasaccharide, namely for linkages A → B, B → C and C → D.

GlcNS,6S ring B and between H4 and H5 of GlcNS,6S ring D (Supplementary data, Figure S6). In addition, some small negative NOEs appeared between H3 and H4 of IdoA,2S ring C, between H3 and H4 of GlcNS,6S ring B and between the H6 protons of both glucosamine rings. In the presence of 5 mol% of IL-10, the heparin tetrasaccharide showed multiple NOEs with negative sign; apart from one single NOE between H2 and H3 of GlcNS,6S ring B, which was positive. The observation of trNOEs clearly indicates an interaction between IL-10 and heparin, which causes an increase of the average correlation time of the ligand and thus a negative NOE. Similar observations were made for the heparin I-S disaccharide too. Here, the sign of the NOE changes from positive in the free state to negative in the presence of IL-10 (Supplementary data, Figure S5).

Structural information of the unbound heparin tetrasaccharide were obtained from ROESY spectra and were compared with NOESY and ROESY spectra of the bound carbohydrate (Supplementary data, Figure S7). In the presence of IL-10, additional NOE cross-peaks were observed between protons H2 of the GlcNS,6S ring B or D and the preceding H1 protons of the 4,5-unsaturated ΔUA,2S ring A or the IdoA,2S ring C, respectively. Furthermore, new cross-peaks were found between proton H2 of GlcNS,6S ring B and protons H3 and H4 of the successive IdoA,2S ring C. Finally, proton H5 of IdoA,2S ring C was involved in two new NOEs to proton H1 of the preceding GlcNS,6S ring B and to H1 within the same IdoA,2S ring C. In principle, those additional NOE signals can represent new intra-molecular contacts in the heparin molecule when bound to IL-10. However, they can also reflect the effect of spin diffusion, which can have significant contributions because of the increased molecular weight of the heparin-IL-10 complex. We cannot absolutely exclude spin diffusion, but we have taken measures to reduce these effects. Transferred NOE experiments were carried out at short mixing times between 50 and 150 ms, at which the buildup curve is in the linear region and contributions from spin diffusion are expected to be small. This was also confirmed by theoretical simulations of the NOESY and ROESY spectra with the program Noemol (Forster and Mulloy 1994). A rotational correlation time of the free heparin of 0.4 ns (Forster and Mulloy 1994) and an averaged correlation time of 1.75 ns for the bound heparin were assumed. As additional control, a trROESY experiment was performed

with heparin in the presence of IL-10 at the same mixing time (150 ms) as for the NOESY experiment. Here, cross-peaks with the same sign as the diagonal signals indicate relayed ROEs, which are caused by spin diffusion. Indeed, the signals mentioned above, which were only present in the NOESY spectrum of bound heparin, showed the same sign as the diagonal peaks (Supplementary data, Figure S7) and were identified to be the result of spin diffusion. Therefore, they were excluded from the NOE distance data used in the following structure calculation.

Heparin structure calculation

We created structural models of heparin based on internal NOE data (Supplementary data, Table SVII and SVIII) by performing simulated annealing MD simulations including hydrogen pair distance restraints. In the unbound case, 42 H–H distance restraints were applied during the simulations (visualized in Supplementary data, Figure S8). A total of 20 showed a deviation from the tolerance interval of <0.2 Å. The ensemble had a structural diversity of 0.37 Å (Figure 7A).

In the bound state, we restrained the distance of 41 hydrogen pairs (visualized in Supplementary data, Figure S8). A total of eight showed a deviation from the tolerance interval of <0.1 Å. The resulting ensemble had a structural diversity of 0.43 Å (Figure 7B).

During the structure calculation, we did not apply experimental constraints involving hydrogens of ring A other than H1 due to inaccurate parameterization of the GLYCAM force field for the 4,5-unsaturated acid ring. Since the $^{4,5}\Delta$-uronic acid ring originates from preparation of the tetrasaccharide by lyase digestion, it plays no functional role for the biology of heparin or HS and, consequently, we do not discuss structural details of this ring – an approach which has been taken from Jin et al. (2009). Hence, functional groups of ring A are not shown in Figure 7.

We quantified the difference in the GAG backbone structure for the bound and unbound case by evaluating the distribution of glycosidic linkage torsional angles in both ensembles (Figure 8). A significant change in the Φ distribution of linkage A → B, a shift in the Ψ distribution of linkage B → C and a significant shift in the Φ distribution of linkage C → D was observed.

The orientation of four of the six sulfate groups in the tetrasaccharide did not differ significantly between the bound and unbound state. The orientation of the 6-O-sulfates of the rings B and D, however, was observed to be affected by the presence of IL-10 (see Supplementary data, Figure S9). The 6-O-sulfate of ring B showed a shift in the rotamer distribution and 10° deviation from the ideal rotation angle of −60°. The 6-O-sulfate of ring D also populated a small fraction of the *gauche–trans* conformer (+60°) in the presence of IL-10. Further information on the conformation of 6-O-sulfate side chains was revealed from ^{3}J couplings between H5 and H6 protons. ^{3}J values for the free tetrasaccharide are: $^{3}J_{H5-H6proR} = 4.3$ Hz and $^{3}J_{H5-H6proS} = 1.9$ Hz for ring B and $^{3}J_{H5-H6proR} = 4.6$ Hz and $^{3}J_{H5-H6proS} = 1.9$ Hz for ring D. Using a general Karplus equation (Haasnoot et al. 1980; Nishida et al. 1988), we determined the C5–C6 bond of both GlcNS,6S rings B and D to have 70% *gauche–gauche* (gg) and 30% *gauche–trans* (gt) conformation, which is similar to the ratio observed for other glucopyranose monosaccharides (Nishida et al. 1988). Unfortunately, exact measurement of H5–H6 couplings for the bound tetrasaccharide molecule was impeded by peak broadening.

Another essential aspect of heparin binding is the role of the conformational equilibrium of the iduronic acid ring. NOEs and scalar couplings are particularly useful to explore this equilibrium. A cross-peak between protons H2 and H5 of IdoA,2S ring C was observed in both, the ROESY spectrum of free heparin and in the trNOESY spectrum of the bound one. This H2–H5 NOE (ROE) is exclusive for the $^{2}S_{o}$ conformer of iduronic acid and incompatible with the $^{1}C_{4}$ form due to a larger distance between both protons (4.0 Å for $^{1}C_{4}$ compared with 2.4 Å for $^{2}S_{o}$; Mulloy et al. 1993). Thus, a considerable content of the $^{2}S_{o}$ conformer is present in the free and in the bound state of the heparin tetrasaccharide. More quantitative information about the conformational equilibrium was obtained from ^{3}J proton–proton couplings. Experimental values for the IdoA,2S ring C (Supplementary data, Table SIX) were compared with computed ^{3}J values of the iduronic acid inside a GlcN,6S-IdoA-OMe disaccharide (Hricovíni and Bízik 2007). According to these data, the $^{1}C_{4} : {}^{2}S_{o}$ ratio for iduronic acid in the heparin tetrasaccharide is 59(±8) % : 41(±8) % in the free state and 33(±4) % : 67(±4) % in the presence of IL-10.

Discussion

Extracellular matrix GAGs play an important role in inflammation and immune responses, e.g., as adhesion points for the extravasion of leucocytes and as carriers of chemokines and growth factors. In the present study, we show that GAGs can bind the cytokine IL-10, which is an important regulator of the adaptive immune system. Using NMR spectroscopy and MD simulations, we investigated the effects of GAG sulfation, size and structure on binding to IL-10.

The studied di- and tetrasaccharides gave generally high and medium STD signals, indicating that all parts of the carbohydrate are positioned in close proximity to IL-10. In particular, the strongest STD effects were found for protons near sulfate groups, i.e., protons H2, H4, H5, H6pro(R) and H6pro(S) of the glucosamine or galactosamine ring, and protons H1, H2 and H3 of the $^{4,5}\Delta$-uronic acid or iduronic acid ring, respectively. This suggests that the sulfate groups are oriented towards the protein surface and that electrostatic interactions are established between GAGs and IL-10. Furthermore, strong STD effects were also obtained for the methyl protons of the acetamide group in the glucosamine and galactosamine. This observation could be attributed to a hydrogen bond of the *N*-amide group or to van der Waals interactions, in which the methyl group could be involved. However, the finding that the non-sulfated HA did not bind IL-10 argues in favor of a major role of GAG sulfation and therefore of the electrostatic interactions. This was also demonstrated by measurement of the binding affinity of different GAG disaccharides with various patterns of sulfation. Here, addition of an extra sulfate group to each possible sulfation position led to a further increase in affinity. In accordance with the observed pattern of STD effects, we conclude that all O- and N-sulfations contribute to IL-10 binding. The relative proportions of N- and O-linked sulfate groups or N-linked acetyl groups can influence GAG interaction with proteins. For example, for heparin binding to basic fibroblast growth factor

(bFGF) (Faham et al. 1996) and monocyte chemoattractant protein 1 (Sweeney et al. 2006) 2-O and N-sulfation were found more important than 6-O-sulfation. However, for other proteins such as IL-8 (Pichert et al. 2012), CXCL12 (Murphy et al. 2007) and HIV-Tat (Rusnati et al. 1997), all O- and N-sulfations are required for GAG binding. In our study, when comparing the individual effects of sulfate groups at certain position, we were not able to find a predominant role of on type of sulfation. Removal of the N-sulfate group almost completely abolished heparin binding. However, this effect is probably caused by the generation of a positively charged amine rather than by the disruption of a direct interaction of the N-sulfate. After all, the triple sulfated heparin and CS showed comparable affinity, although the N-sulfate is absent in the latter disaccharide.

In contrast to the degree of sulfation, monosaccharide conformation and glycosidic linkage geometry appear to have limited influence on IL-10-GAG binding. Comparing heparin and CS disaccharides with the same sulfation level, similar K_D values were obtained. It should be noted that naturally occurring CS is mostly monosulfated at position O4 or O6. The corresponding disaccharides showed 30- to 60-fold less affinity than the fully sulfated heparin disaccharide. Nevertheless, there also exists highly sulfated CS, e.g., CS-E type that was shown to be important for growth factor binding and brain development (Deepa et al. 2002; Purushothaman et al. 2007).

Disaccharides were used successfully for the identification of GAG-binding sites in other proteins (Murphy et al. 2007) but have some limitations as GAG model. On the one hand, they cover only a short part of the GAG polymer and the 4,5-unsaturated uronic acid has a distorted ring conformation different from the $^{1}C_{4}$ chair or $^{2}S_{o}$ skew-boat conformation of iduronic acid or the $^{4}C_{1}$ structure of glucuronic acid. On the other hand, we observed pronounced STD effects already for disaccharides showing that small GAGs make already considerable interactions with the protein. Furthermore, in ^{1}H–^{15}N HSQC spectra of IL-10, chemical shift perturbations were found for the same range of amino acids as in the presence of longer oligosaccharides (Supplementary data, Figure S1). This finding indicates that the disaccharide already occupies the same binding region as longer GAG carbohydrates, which was demonstrated also for other GAG-binding proteins, e.g., acidic fibroblast growth factor (aFGF) (Liu et al. 2008) and CXCL12 (Murphy et al. 2007). We therefore conclude that binding properties studied exemplarily on disaccharides here apply also for GAG oligosaccharides.

IL-10 is rich in basic amino acids capable of forming salt bridges with GAGs. The human monomeric protein contains 9 Arg and 13 Lys residues. In particular, there is a cluster of 5 Arg involving amino acids 101–111 (LRLRLRRCHRF) at the C-terminal end of helix D and the adjacent DE loop. This region is highly conserved among different species and appears to be a specific feature of IL-10. We calculated IL-10's Coulomb potential and evaluated its topology in space as previously described in Samsonov et al. (2014). Based on these data, we can indeed predict a GAG-binding site in the named region (for details, see Supplementary data, Figure S10). For symmetry reasons, this region occurs twice in the IL-10 dimer, separated by a distance of ~30–40 Å that is comparable with the length of an extended GAG decasaccharide. Based on our STD binding data, we hypothesize a scenario in which an appropriately long GAG molecule could bridge both binding sites. For a fully sulfated heparin octa- or decasaccharide binding affinity is nearly 10- or 20-fold higher than for the heparin disaccharide I-S. We interpret this increase in affinity as effect of positive cooperativity indicated by a steeper slope of the corresponding binding curves and a Hill coefficient of ~2. Once the GAG molecule is fixed to one binding site, association with the second site can happen very fast, e.g., due to spatial restriction and thus affinity is also increased.

GAG conformation and flexibility were exemplarily studied for a heparin tetrasaccharide in its bound and unbound form. Heparin mimics the highly sulfated S-domains of HS and can thus provide a model for extracellular matrix GAGs. Furthermore, heparin contains an iduronic acid, whose crucial role for the structure of heparin itself and for protein–GAG interaction is widely recognized (Canales et al. 2005; Angulo et al. 2005; Jin et al. 2009). That property together with its high sulfation degree as prerequisite for IL-10 binding makes heparin an interesting GAG model. The length of a tetrasaccharide represents thereby a compromise between a short GAG sequence which can still reflect the native polymer structure and the accessibility of heparin for characterization by high-resolution NMR spectroscopy. For heparin longer than a tetrasaccharide, distinction of trNOEs arising from the bound or unbound form was no longer possible.

The NOE distance data and MD simulations have led to proper heparin structure models. In both, the bound and unbound case, the ensemble representatives have their rings in valid conformations, namely ring B in $^{4}C_{1}$, ring C in $^{2}S_{o}$ and ring D in $^{4}C_{1}$ conformation. Also the distribution of glycosidic linkage torsional angles is in a valid range of values, as observed in free heparin microsecond MD simulations (data not shown) and in bound and unbound heparin structures found in the PDB.

The generated structure models let us conclude that the bound heparin structure is less bent than its free form. The small but significant difference observed in the backbone structure of the bound and unbound ensembles is reflected by their glycosidic linkage torsional angle distributions. However, although glycosidic bond angles between the free and bound state do vary between 10° and 30° for linkages A → B and C → D, the overall tetrasaccharide conformation is maintained and is consistent with the helical structure of the heparin dodecasaccharide previously observed by NMR and modeling (Mulloy et al. 1993). Also in the high-affinity complex between bFGF and a heparin tetrasaccharide (Faham et al. 1996; Mikhailov et al. 1996) the backbone differences relative to the unbound GAG are rather small and provide no indication about the interaction strength. Furthermore, according to our heparin structure models, the orientation of most functional groups of rings B, C and D is conserved among the bound and unbound MD ensembles. Notable exceptions are the positions of the 6-O-sulfate groups of rings B and D. In ring B, the 6-O-sulfate is only in *gauche–gauche*, but there is a slight shift by about −10° of the rotamer distribution in the bound heparin structure. In ring C, an additional fraction of the *gauche–trans* conformer in the presence of IL-10 is observed. The observation of the 6-O-sulfate being mostly in *gauche–gauche* orientation is in contradiction to our ^{3}J coupling analysis. The latter estimated the C5–C6 bond in both glucosamine residues to have 70% *gauche–gauche* and 30% *gauche–trans* character as found for other D-glucopyranoses (Nishida et al. 1988). The described

contradiction suggests that the sulfate rotamer distribution as yielded by our MD structure optimization protocol is oversensitive to small variations in single distance restraints and that the interpretation of the ^3J coupling data should take precedence.

The conformation of heparin sulfated iduronic acid in complex with proteins has been widely studied. Iduronate may exist in ^2S_o, $^1C_4$ or as mixture of both conformations in heparin–protein complexes depending on specificity of the receptor binding site or predominance of one conformer in solution. In the crystal structure of the bFGF–heparin complex, the IdoA,2S ring makes several contacts with the protein and resides in a $^1C_4$ chair (Faham et al. 1996). If the heparin chain is elongated, as for the heparin hexasaccharide–bFGF complex, the second IdoA,2S ring makes fewer interactions and adopts a ^2S_o structure. In contrast to bFGF, it has been reported that aFGF recognizes both conformations of iduronic acid in a heparin hexasaccharide. $^1C_4$ and ^2S_o were nearly equally populated as estimated from characteristic NOE intensities of both forms (Canales et al. 2005). In our heparin models, the IdoA,2S ring C has a clear preference towards ^2S_o, whereas the ^3J couplings indicate a simultaneous presence of both chair and skew-boat structure. That discrepancy probably originates from the strong H2–H5 NOE, which is dominated by the shorter H2–H5 distance of the ^2S_o structure (2.4 Å) compared with the $^1C_4$ form (4.0 Å) (Mulloy et al. 1993) and thus fixes the monosaccharide in skew-boat conformation during the simulation. In contrast, based on ^3J couplings, we determined the equilibrium between $^1C_4$ and ^2S_o in the IL-10-bound structure to be 33%:67%. This interesting observation can indicate that either the iduronic acid is not interacting with the protein, and thus interconversion of the sugar ring can take place, or two binding modes may exist – one with the iduronic acid bound in $^1C_4$ and the other with the iduronate in ^2S_o. For some heparin–protein complexes also a conformational selection mechanism has been previously suggested. For example, in the crystal structure of annexin V with two heparin tetrasaccharide molecules the IdoA,2S ring of molecule 2, which interacts with the protein, adopts a ^2S_o conformation, whereas the non-interacting IdoA,2S ring in the second molecule resides in the $^1C_4$ conformation (Capila et al. 2001).

In conclusion, we show that IL-10 is capable of binding a variety of GAG ligands for which we determined protons that are in close proximity to the protein. This molecular recognition imposes only minor changes on the overall GAG structure. We find that the interaction strength is highly dependent on GAG sulfation degree, whereas sulfation position seems to have minor importance. Our results provide information on the interaction properties of GAGs and IL-10 and shed light on a functional role of GAGs in IL-10 biology. Similar to their role in regulating the receptor interaction of other cytokines and growth factors (Schlessinger et al. 2000), GAGs could influence IL-10 receptor binding as well. An inhibition of IL-10 signaling by GAGs was demonstrated but the mechanism remains so far unknown. Considering the fact that interaction with the IL-10 receptor 2 chain (IL-10R2) is very low (ca. 200 μM) (Yoon et al. 2006), GAGs could easily compete for receptor binding and inhibit the formation of the ternary signaling complex. Affinity of the heparin I-S disaccharide is comparable with IL-10R2 and the binding strength of longer GAGs is even higher. Identification of the GAG-binding site of IL-10 will therefore help to better understand by which mechanism GAGs could deteriorate receptor interaction.

Moreover, cell surface or extracellular matrix GAGs can also serve to immobilize IL-10 in the microenvironment of a releasing cell and to produce high local concentrations of the cytokine. In fact, in vivo functions of IL-10 are rather restricted to the vicinity of the IL-10 producing cell and endocrine effects over long distances or through the blood circulation are suggested to have minor importance (Roers and Müller 2008; Sabat et al. 2010). Interestingly, IL-10 from different cellular sources was observed to have distinct functionalities (Roers and Müller 2008). Differences in GAG expression levels and profiles with respect to, e.g., sulfation degree or position could lead to different extents of IL-10 immobilization for which our results can provide a mechanistic explanation.

Furthermore, the characterized binding properties can be taken into account for the design of tissue-like matrix materials in regenerative medicine. Those matrices can be modified with GAGs as extracellular matrix mimetic and loaded with regulatory proteins that are delivered in a controlled manner after implantation to assist healing processes (Lee and Shin 2007; Dvir et al. 2011). IL-10 for instance can be loaded on such matrices and then be applied for locally down-regulating inflammatory processes.

Supplementary data

Supplementary data for this article are available online at http://glycob.oxfordjournals.org/.

Conflict of interest statement

None declared.

Funding

This work was supported by the Deutsche Forschungsgemeinschaft (Transregio-SFB 67, A6 and A7) and grants from the Studienstiftung des deutschen Volkes (J.P.G.) and the Stipendienfonds der Chemischen Industrie e.V. (G.K.).

Acknowledgements

We thank Professor Jörg Matysik (Analytical Chemistry/University of Leipzig) who kindly provided access to the 700 MHz NMR spectrometer. We are grateful to the ZIH at TU Dresden for providing high-performance computational resources.

Abbreviations

aFGF, acidic fibroblast growth factor; bFGF, basic fibroblast growth factor; CS, chondroitin sulfate; DS, dermatan sulfate; DSS, 2,2-dimethyl-2-silapentene-5-sulfonate; GAG, glycosaminoglycan; HS, heparan sulfate; HSQC, heteronuclear single quantum coherence; HA, hyaluronan; MD, molecular dynamics; NMR, nuclear magnetic resonance; NOE, nuclear Overhauser effect; NOESY, nuclear Overhauser effect spectroscopy; ROESY, rotating-frame nuclear Overhauser effect

spectroscopy; SDS-PAGE, sodium dodecyl sulfate polyacrylamide gel electrophoresis; STD, saturation transfer difference; STD-AF, STD amplification factor; TOCSY, total correlation spectroscopy.

References

Angulo J, Enriquez-Navas PM, Nieto PM. 2010. Ligand-receptor binding affinities from saturation transfer difference (STD) NMR spectroscopy: The binding isotherm of STD initial growth rates. *Chemistry*. 16:7803–7812.

Angulo J, Hricovini M, Gairi M, Guerrini M, de Paz JL, Ojeda R, Martin-Lomas M, Nieto PM. 2005. Dynamic properties of biologically active synthetic heparin-like hexasaccharides. *Glycobiology*. 15:1008–1015.

Ball C, Vigues S, Gee CK, Poole S, Bristow AF. 2001. Rat interleukin-10: Production and characterisation of biologically active protein in a recombinant bacterial expression system. *Eur Cytokine Netw*. 12:187–193.

Bax A, Davis DG. 1985. MLEV-17-based two-dimensional homonuclear magnetization transfer spectroscopy. *J Magn Reson*. 65:355–360.

Canales A, Angulo J, Ojeda R, Bruix M, Fayos R, Lozano R, Gimenez-Gallego G, Martin-Lomas M, Nieto PM, Jimenez-Barbero J. 2005. Conformational flexibility of a synthetic glycosylaminoglycan bound to a fibroblast growth factor. FGF-1 recognizes both the $^{1}C_{4}$ and $^{2}S_{o}$ conformations of a bioactive heparin-like hexasaccharide. *J Am Chem Soc*. 127:5778–5779.

Capila I, Hernaiz MJ, Mo YD, Mealy TR, Campos B, Dedman JR, Linhardt RJ, Seaton BA. 2001. Annexin V-heparin oligosaccharide complex suggests heparan sulfate-mediated assembly on cell surfaces. *Structure*. 9:57–64.

Case DA, Darden TA, Cheatham TEI, Simmerling CL, Wang J, Duke RE, Luo R, Walker RC, Zhang W, Merz KM, et al. 2012. *AMBER 12*. San Francisco: University of California.

Clarke D, Katoh O, Gibbs RV, Griffiths SD, Gordon MY. 1995. Interaction of interleukin-7 (IL-7) with glycosaminoglycans and its biological relevance. *Cytokine*. 7:325–330.

D'Amore PA. 1990. Heparin-endothelial cell interactions. *Haemostasis*. 20 (Suppl. 1):159–165.

Deepa SS, Umehara Y, Higashiyama S, Itoh N, Sugahara K. 2002. Specific molecular interactions of oversulfated chondroitin sulfate E with various heparin-binding growth factors. Implications as a physiological binding partner in the brain and other tissues. *J Biol Chem*. 277:43707–43716.

Dvir T, Timko BP, Kohane DS, Langer R. 2011. Nanotechnological strategies for engineering complex tissues. *Nat Nanotechnol*. 6:13–22.

Esko JD, Linhardt RJ. 2009. Proteins that bind sulfated glycosaminoglycans. In: Varki A, Cummings RD, Esko JD, editors. *Essentials of Glycobiology*. 2nd ed. Cold Spring Harbor (NY): Cold Spring Harbor Laboratory Press. p. 501–512.

Faham S, Hileman RE, Fromm JR, Linhardt RJ, Rees DC. 1996. Heparin structure and interactions with basic fibroblast growth factor. *Science*. 271:1116–1120.

Fiorentino DF, Bond MW, Mosmann TR. 1989. Two types of mouse T helper cell IV. Th2 clones secrete a factor that inhibits cytokine production by Th1 clones. *J Exp Med*. 170:2081–2095.

Fleming SD, Campbell PA. 1996. Macrophages have cell surface IL-10 that regulates macrophage bactericidal activity. *J Immunol*. 156:1143–1150.

Forster MJ, Mulloy B. 1994. Rationalizing nuclear overhauser effect data for compounds adopting multiple-solution conformations. *J Comp Chem*. 15:155–161.

Gallagher JT. 1989. The extended family of proteoglycans: Social residents of the pericellular zone. *Curr Opin Cell Biol*. 1:1201–1218.

Gallagher JT. 1997. Structure-activity relationship of heparan sulphate. *Biochem Soc Trans*. 25:1206–1209.

Gallagher JT, Turnbull JE. 1992. Heparan sulfate in the binding and activation of basic fibroblast growth factor. *Glycobiology*. 2:523–528.

Gallagher JT, Turnbull JE, Lyon M. 1990. Heparan sulphate proteoglycans. *Biochem Soc Trans*. 18:207–209.

Gandhi NS, Mancera RL. 2008. The structure of glycosaminoglycans and their interactions with proteins. *Chem Biol Drug Des*. 72:455–482.

Haasnoot CAG, Deleeuw FAAM, Altona C. 1980. Prediction of *anti* and *gauche* vicinal proton-proton coupling-constants for hexapyranose rings using a generalized Karplus equation. *Bull Soc Chim Belg*. 89:125–131.

Handel TM, Johnson Z, Crown SE, Lau EK, Sweeney M, Proudfoot AE. 2005. Regulation of protein function by glycosaminoglycans—as exemplified by chemokines. *Annu Rev Biochem*. 74:385–410.

Hricovíni M, Bízik F. 2007. Relationship between structure and three-bond proton-proton coupling constants in glycosaminoglycans. *Carbohydr Res*. 342:779–783.

Jin L, Hricovini M, Deakin JA, Lyon M, Uhrin D. 2009. Residual dipolar coupling investigation of a heparin tetrasaccharide confirms the limited effect of flexibility of the iduronic acid on the molecular shape of heparin. *Glycobiology*. 19: 1185–1196.

Johnson Z, Proudfoot AE, Handel TM. 2005. Interaction of chemokines and glycosaminoglycans: A new twist in the regulation of chemokine function with opportunities for therapeutic intervention. *Cytokine Growth Factor Rev*. 16:625–636.

Kay LE, Keifer P, Saarinen T. 1992. Pure absorption gradient enhanced heteronuclear single quantum correlation spectroscopy with improved sensitivity. *J Am Chem Soc*. 114:10663–10665.

Kirschner KN, Yongye AB, Tschampel SM, Gonzalez-Outeirino J, Daniels CR, Foley BL, Woods RJ. 2008. GLYCAM06: A generalizable biomolecular force field. Carbohydrates. *J Comput Chem*. 29:622–655.

Künze G, Theisgen S, Huster D. 2013. Backbone ^{1}H, ^{15}N, ^{13}C and side chain $^{13}C\beta$ NMR chemical shift assignment of murine interleukin-10. *Biomol NMR Assign*, doi: 10.1007/s12104-013-9521-3.

Lee SH, Shin H. 2007. Matrices and scaffolds for delivery of bioactive molecules in bone and cartilage tissue engineering. *Adv Drug Deliv Rev*. 59:339–359.

Li W, Johnson DJ, Esmon CT, Huntington JA. 2004. Structure of the antithrombin-thrombin-heparin ternary complex reveals the antithrombotic mechanism of heparin. *Nat Struct Mol Biol*. 11:857–862.

Liu L, Bytheway I, Karoli T, Fairweather JK, Cochran S, Li C, Ferro V. 2008. Design, synthesis, FGF-1 binding, and molecular modeling studies of conformationally flexible heparin mimetic disaccharides. *Bioorg Med Chem Lett*. 18:344–349.

Liu M, Mao X, Ye C, Huang H, Nicholson JK, Lindon JC. 1998. Improved WATERGATE pulse sequences for solvent suppression in NMR spectroscopy. *J Magn Reson*. 132:125–129.

Mayer M, Meyer B. 2001. Group epitope mapping by saturation transfer difference NMR to identify segments of a ligand in direct contact with a protein receptor. *J Am Chem Soc*. 123:6108–6117.

Mikhailov D, Mayo KH, Vlahov IR, Toida T, Pervin A, Linhardt RJ. 1996. NMR solution conformation of heparin-derived tetrasaccharide. *Biochem J*. 318(Pt 1):93–102.

Moore KW, O'Garra A, de Waal MR, Vieira P, Mosmann TR. 1993. Interleukin-10. *Annu Rev Immunol*. 11:165–190.

Mulloy B, Forster MJ, Jones C, Davies DB. 1993. NMR and molecular-modelling studies of the solution conformation of heparin. *Biochem J*. 293 (Pt 3):849–858.

Murphy JW, Cho Y, Sachpatzidis A, Fan CP, Hodsdon ME, Lolis E. 2007. Structural and functional basis of CXCL12 (strornal cell-derived factor-1α) binding to heparin. *J Biol Chem*. 282:10018–10027.

Nishida Y, Hori H, Ohrui H, Meguro H. 1988. ^{1}H NMR analyses of rotameric distribution of C5-C6 bonds of D-glucopyranoses in solution. *J Carbohydr Chem*. 7:239–250.

Pichert A, Samsonov SA, Theisgen S, Thomas L, Baumann L, Schiller J, Beck-Sickinger AG, Huster D, Pisabarro MT. 2012. Characterization of the interaction of interleukin-8 with hyaluronan, chondroitin sulfate, dermatan sulfate and their sulfated derivatives by spectroscopy and molecular modeling. *Glycobiology*. 22:134–145.

Pratta MA, Yao W, Decicco C, Tortorella MD, Liu RQ, Copeland RA, Magolda R, Newton RC, Trzaskos JM, Arner EC. 2003. Aggrecan protects cartilage collagen from proteolytic cleavage. *J Biol Chem*. 278:45539–45545.

Prydz K, Dalen KT. 2000. Synthesis and sorting of proteoglycans. *J Cell Sci*. 113(Pt 2):193–205.

Purushothaman A, Fukuda J, Mizumoto S, ten Dam GB, van Kuppevelt TH, Kitagawa H, Mikami T, Sugahara K. 2007. Functions of chondroitin sulfate/dermatan sulfate chains in brain development. Critical roles of E and iE disaccharide units recognized by a single chain antibody GD3G7. *J Biol Chem*. 282:19442–19452.

Roberts R, Gallagher J, Spooncer E, Allen TD, Bloomfield F, Dexter TM. 1988. Heparan sulphate bound growth factors: A mechanism for stromal cell mediated haemopoiesis. *Nature*. 332:376–378.

Roers A, Müller W. 2008. Distinct functions of interleukin-10 derived from different cellular sources. *Curr Immunol Rev*. 4:37–42.

Rusnati M, Coltrini D, Oreste P, Zoppetti G, Albini A, Noonan D, dda di FF, Giacca M, Presta M. 1997. Interaction of HIV-1 Tat protein with heparin. Role of the backbone structure, sulfation, and size. *J Biol Chem*. 272: 11313–11320.

Sabat R, Grutz G, Warszawska K, Kirsch S, Witte E, Wolk K, Geginat J. 2010. Biology of interleukin-10. *Cytokine Growth Factor Rev*. 21:331–344.

Sadir R, Imberty A, Baleux F, Lortat-Jacob H. 2004. Heparan sulfate/heparin oligosaccharides protect stromal cell-derived factor-1 (SDF-1)/CXCL12 against proteolysis induced by CD26/dipeptidyl peptidase IV. *J Biol Chem*. 279:43854–43860.

Salek-Ardakani S, Arrand JR, Shaw D, Mackett M. 2000. Heparin and heparan sulfate bind interleukin-10 and modulate its activity. *Blood*. 96: 1879–1888.

Samsonov SA, Gehrcke J-P, Pisabarro MT. 2014. Flexibility and explicit solvent in molecular-dynamics-based docking of protein-glycosaminoglycan systems. *J Chem Inf Model*. 54:582–592.

Schlessinger J, Plotnikov AN, Ibrahimi OA, Eliseenkova AV, Yeh BK, Yayon A, Linhardt RJ, Mohammadi M. 2000. Crystal structure of a ternary FGF-FGFR-heparin complex reveals a dual role for heparin in FGFR binding and dimerization. *Mol Cell*. 6:743–750.

Schleucher J, Schwendinger M, Sattler M, Schmidt P, Schedletzky O, Glaser SJ, Sorensen OW, Griesinger C. 1994. A general enhancement scheme in heteronuclear multidimensional NMR employing pulsed field gradients. *J Biomol NMR*. 4:301–306.

Shaka AJ, Barker PB, Freeman R. 1985. Computer-optimized decoupling scheme for wideband applications and low-level operation. *J Magn Reson*. 64:547–552.

Sweeney MD, Yu Y, Leary JA. 2006. Effects of sulfate position on heparin octasaccharide binding to CCL2 examined by tandem mass spectrometry. *J Am Soc Mass Spectrom*. 17:1114–1119.

Tan JC, Braun S, Rong H, DiGiacomo R, Dolphin E, Baldwin S, Narula SK, Zavodny PJ, Chou CC. 1995. Characterization of recombinant extracellular domain of human interleukin-10 receptor. *J Biol Chem*. 270:12906–12911.

Wider G, Macura S, Kumar A, Ernst RR, Wuthrich K. 1984. Homonuclear two-dimensional ^{1}H NMR of proteins. Experimental procedures. *J Magn Reson*. 56:207–234.

Yoon SI, Logsdon NJ, Sheikh F, Donnelly RP, Walter MR. 2006. Conformational changes mediate interleukin-10 receptor 2 (IL-10R2) binding to IL-10 and assembly of the signaling complex. *J Biol Chem*. 281:35088–35096.

Zdanov A. 2004. Structural features of the interleukin-10 family of cytokines. *Curr Pharm Des*. 10:3873–3884.